Published in final edited form as:
J Am Chem Soc. 2010 January 13; 132(1): 67–69. doi:10.1021/ja908467y.

Optical Imaging of Mammary and Prostate Tumors in Living Animals using a Synthetic Near Infrared Zinc(II)-Dipicolylamine Probe for Anionic Cell Surfaces

Bryan A. Smith[1], **Walter J. Akers**[2], **W. Matthew Leevy**[1], **Andrew J. Lampkins**[1], **Shuzhang Xiao**[1], **William Wolter**[3], **Mark A. Suckow**[3], **Samuel Achilefu**[2], and **Bradley D. Smith**[1,*]

[1] Department of Chemistry and Biochemistry, 251 Nieuwland Science Hall, University of Notre Dame, Notre Dame, IN 46556

[2] Department of Radiology, Washington University School of Medicine, 4525 Scott Ave, St. Louis, MO 63110

[3] Freimann Life Science Center, 400 Galvin Life Science, University of Notre Dame, Notre Dame, IN 46556

Abstract

In vivo optical imaging shows that a fluorescent imaging probe, comprised of a near-infrared fluorophore attached to an affinity group containing two zinc(II)-dipicolylamine (Zn-DPA) units, targets prostate and mammary tumors in two different xenograft animal models. The tumor selectivity is absent with control fluorophores whose structures do not have appended Zn-DPA targeting ligands. Ex vivo biodistribution and histological analyses indicate that the probe is targeting the necrotic regions of the tumors, which is consistent with in vitro microscopy showing selective targeting of the anionic membrane surfaces of dead and dying cells.

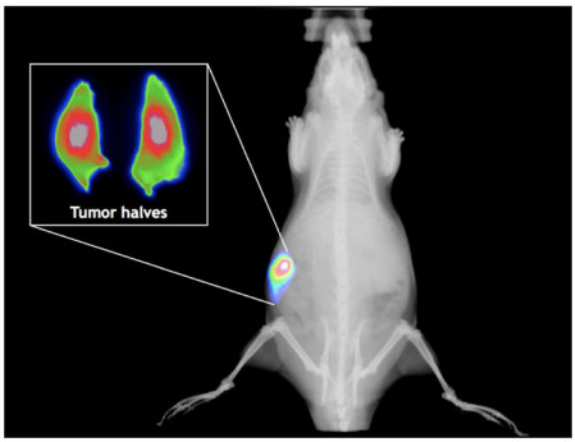

There is a major ongoing research effort to identify oligonucleotide and protein biomarkers of malignant disease.[1] Phospholipid biomarkers are less common, however, there is increasing evidence that the membrane surfaces of certain cells and particles of biomedical significance,

smith.115@nd.edu.

Supporting Information Available: Experimental details and additional imaging data. The information is available free of charge via the Internet at http://pubs.acs.org.

such as apoptotic cells,[2] activated cells,[3] tumor vasculature,[4] microvesicles,[5] bacteria,[6] and viruses,[7] expose unusually high levels of negatively charged phospholipids. Proteins and antibodies that can selectively target these anionic membrane surfaces and distinguish them from the near-neutral membrane surfaces of normal human cells have promising potential as imaging probes,[8] drug delivery agents,[9] and targeted molecular therapeutics.[10] Notable examples are the protein, Annexin V, which is under clinical investigation as an imaging probe for dead/dying tissue,[11] and the antibody, Bavituximab, which targets viruses and tumor vasculature.[12] It is often challenging to optimize the formulation and pharmaceutical properties of proteins, thus, there is a need to develop small molecule mimics of these proteins that exhibit the same targeting capabilities.[13]

Synthetic zinc(II)-dipicolylamine (Zn-DPA) coordination complexes are known to associate with multianionic phosphorylated biomolecules,[14] and we have discovered that they can be converted into optical imaging probes that target the outer surfaces of anionic vesicle and cell membranes.15 Fluorescent Zn-DPA probes can distinguish dead and dying mammalian cells from healthy cells in a cell culture,16 and also selectively target bacteria in heterogeneous biological media.17 Furthermore, we have recently demonstrated that the near-IR fluorescent probe **1** can be used to image bacterial infections in living mice,[18] indicating that probe **1** has a notable ability to selectively target anionic cells over other anionic sites in the bloodstream and extracellular matrix. Here, we greatly expand the animal imaging capability of probe **1** by showing that it can also target the anionic dead and dying cells within xenograft tumors in rat and mouse models. The structure of probe **1** includes a near-IR carbocyanine fluorophore whose absorption and emission wavelengths of 794 and 810 nm, respectively, are within the optimal window for maximum penetration through skin and tissue.[19] The high tumor selectivity of **1** is demonstrated by comparison to the less-selective imaging that is achieved by using control near-IR fluorophores **2** and **3** whose structures do not have Zn-DPA targeting ligands.[20]

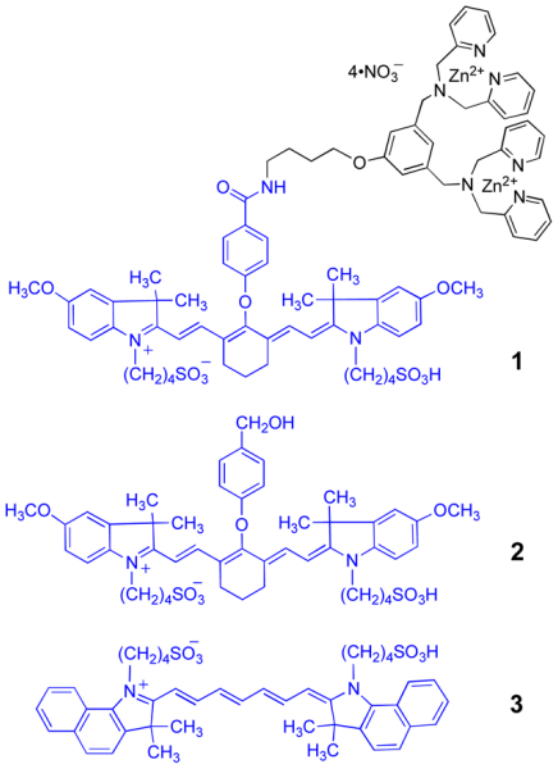

The expected ability of probe **1** to selectively target dead and dying cells with exposed anionic phosphatidylserine was confirmed with in vitro fluorescence microscopy studies of mammalian cells treated with a cytotoxic agent.[16] Specifically, treatment of Jurkat cells (T lymphocytes) with camptothecin induced significant amounts of cell death, and as shown in Figure 1, the near-IR probe **1** stained the same cells as fluorescently labeled Annexin V. Using procedures that were approved by the appropriate institutional animal care and use committee, two tumor bearing animal models were selected for in vivo imaging: 1) immunocompetent Lobund Wistar rats with PAIII prostate tumors,[21] and 2) athymic nude mice containing EMT-6 mammary tumors.[22] These two tumor models were chosen, in part, because they develop foci of necrotic cells, especially in the tumor cores. A typical imaging study of the rat prostate tumor model employed three cohorts of rats with 1×10^6 PAIII cells injected subcutaneously in the right flank. The tumors grew over approximately 14 days followed by intravenous injection of either probe **1**, **2**, or **3** (3.0 mg/kg). The rats were anesthetized and placed in a whole-body, small animal imaging station that was configured for epifluorescence imaging.[23] Each animal was illuminated with filtered light at 750 ± 10 nm and the emission intensity was collected at 830 ± 20 nm. In addition, a co-registered X-ray image was acquired. Clearance of the probes from the blood streams of the living animals was monitored by imaging at regular 3-hour intervals. In the case of probe **1**, there was clear evidence for selective accumulation in the tumor after 24 hrs (Figure 2A). A region of interest analysis compared the tumor signal intensity with the signal from the same area of skin on the opposite side of the rat, to give a target to non-target ratio (T/NT). At the 24 hr time point, the average T/NT for the cohort treated with probe **1** was 2.2 and about twice that for control fluorohores **2** and **3**. The rats were then sacrificed and their tissues harvested for ex vivo analysis of probe biodistribution. Fluorescence intensity images of the excised tissues confirmed the relatively high tumor selectivity of probe **1** (see Supporting Information). The bar graph in Figure 2B shows that average tumor targeting with probe **1** was 36-fold higher than control **2** and also much higher than control **3**.[24] The spatial distribution of probe **1** within the resected tumors was determined by slicing them in half along the longest axis. Fluorescence imaging of the interior-facing surfaces of these tumor halves revealed that probe **1** was not distributed uniformly, with the highest fluorescence intensities coming from the core of the tumors (Figure 3A). Additional microscopic imaging of histological slices showed that the near-IR fluorescence from **1** colocalized with the tumor's necrotic regions (compare Figures 3B and 3C, and see Supporting Information for additional histological analyses).

The ability of **1** to target and identify tumors in vivo was further tested using a mouse EMT-6 mammary tumor model. In a typical study, two cohorts of NCRNU nude mice were subcutaneously injected with 1×10^5 EMT-6 mammary carcinoma cells in the right shoulder. After 10 days, the tumors were palpable, and probe **1** or control **2** (3.0 mg/kg) was injected intravenously into the mice via the tail vein. As before, fluorescence imaging was used to monitor clearance of the probes from the blood streams of the living animals. The in vivo image in Figure 4 shows a typical tumor bearing mouse at 24 hrs post-administration of probe **1**. The average T/NT ratio for the cohort treated with probe **1** was 70% greater than T/NT for control **2** (see Supporting Information). As with the rat prostate tumor model, ex vivo imaging of the excised mouse tissues showed that average tumor selectivity for probe **1** was almost 18-fold higher than control **2**.[24] Again, the tumors were sliced in half and fluorescence imaging showed that the probe localized towards the interior of the tumors. Confirmation that the tumor cores contained significant regions of dead/dying tissue was gained by TUNEL analysis of histological slices.

In summary, the synthetic fluorescent near-IR imaging probe **1** with an appended Zn-DPA affinity ligand, can selectively accumulate in prostate and mammary tumors in two different xenograft animal models. Ex vivo biodistribution and histological analyses suggest that probe **1** targets the necrotic regions of the tumors,[25] which is consistent with in vitro microscopy

showing selective targeting of the anionic membrane surfaces of dead and dying cells. Imaging probes that can determine, non-invasively, the amount and type of cell death in tumors may have utility in clinical prognosis of tumor pathogenesis.[26] Future studies will evaluate if probe **1** can be used to non-invasively monitor tumor cell death due to anticancer therapy.[27] It should also be possible to produce analogous Zn-DPA probes with reporter groups that allow deep tissue imaging of cancer in humans.[28]

Supplementary Material

Refer to Web version on PubMed Central for supplementary material.

Acknowledgments

We thank Ms. Valerie Sailes for histological analyses. This work was supported by Walther Cancer Center, the Notre Dame Integrated Imaging Facility, and NIH grants R01GM059078 (B.D.S.), T32GM075762 (B.A.S.).

References

1. Kulasingam V, Diamandis EP. Nat Clin Pract Oncol 2008;5:588–599. [PubMed: 18695711]
2. Hoffman PR, deCathelineau AM, Ogden CA, Leverrier Y, Bratton DL, Daleke DL, Ridley AJ, Fadok VA, Henson PM. J Cell Biol 2001;155:649–659. [PubMed: 11706053]
3. Elliot JI, Surprenant A, Marelli-Berg FM, Cooper JC, Cassady-Cain RL, Wooding C, Linton K, Alexander DR, Higgins CF. Nat Cell Biol 2005;8:808–816.
4. Ran S, Downes A, Thorpe PA. Cancer Res 2002;62:6132–6140. [PubMed: 12414638]
5. Distler JHW, Huber LC, Reich CF III, Gay S, Distler O, Pisetsky DS. Apoptosis 2005;10:731–741. [PubMed: 16133865]
6. Epand RM, Epand RF. Mol Biosys 2009;5:580–587.
7. Mercer J, Helenius A. Science 2008;320:531–535. [PubMed: 18436786]
8. (a) Jennewein M, Lewis MA, Zhao D, Tsyganov E, Slavine N, He J, Watkins L, Kodibagkar VD, O'Kelly S, Kulkarni P, Antich PP, Hermanne A, Rosch F, Mason RP, Thorpe PE. Clin Cancer Res 2008;14:1377–1385. [PubMed: 18316558] (b) Krishnan AS, Neves AA, de Backer MM, Hu DE, Davletov B, Kettunen MI, Brindle KM. Radiology 2008;246:854–862. [PubMed: 18187402]
9. Kenis H, Hofstra L, Reutelingsperger CPM. Cell Mol Life Sci 2007;64:2859–2862. [PubMed: 17876516]
10. Ran S, He J, Huang X, Soares M, Scothorn D, Thorpe PE. Clin Cancer Res 2005;11:1551–1562. [PubMed: 15746060]
11. (a) Boersma HH, Kietselar BLJH, Stolk LML, Bennaghmouch A, Hofstra L, Narula J, Heidendal GAK, Reutelingsperger CPM. J Nucl Med 2005;46:2035–2050. [PubMed: 16330568] (b) Blankenberg FG. Cancer Biol Ther 2008;7:1–8. [PubMed: 18614860]
12. (a) Soares MM, King SW, Thorpe PE. Nature Med 2008;14:1357–1362. [PubMed: 19029986] (b) Huang X, Bennett M, Thorpe PE. Cancer Res 2005;65:4408–4416. [PubMed: 15899833]
13. (a) Lambert TN, Smith BD. Coord Chem Rev 2003;240:129–141. (b) Hanshaw RG, Stahelin RV, Smith BD. Chem Eur J 2008;14:1690–1697.
14. For recent reviews of molecular recognition using Zn-DPA complexes, see: (a) Sakamoto T, Ojida A, Hamachi I. Chem Commun 2009:141–152. (b) Kim SK, Lee DH, Hong JI, Yoon J. Acc Chem Res 2009;42:23–31. [PubMed: 18798656] (b) Kruppa M, König B. Chem Rev 2006;106:3520–3560. [PubMed: 16967915]
15. (a) Hanshaw RG, Smith BD. Bioorg Med Chem 2005;13:5035–5042. [PubMed: 15914007] (b) O'Neil EJ, Smith BD. Coord Chem Rev 2006;250:3068–3080.
16. (a) Hanshaw RG, Lakshmi C, Lambert TN, Johnson JR, Smith BD. ChemBioChem 2005;12:2214–2220. [PubMed: 16276499] (b) DiVittorio KM, Johnson JR, Johansson E, Reynolds AJ, Jolliffe KA, Smith BD. Org Biomol Chem 2006;4:1966–1976. [PubMed: 16688342] (c) Koulov AV, Stucker K, Lakshmi C, Robinson JP, Smith BD. Cell Death Diff 2003;10:1357–1359. (d) Koulov AV, Hanshaw

RG, Stucker KA, Lakshmi C, Smith BD. Isr J Chem 2005;45:373–379. (e) Quinti L, Weissleder R, Tung CH. Nano Lett 2006;6:488–490. [PubMed: 16522048]

17. Leevy WM, Johnson JR, Lakshmi C, Morris J, Marquez M, Smith BD. Chem Commun 2006:1595–1597.
18. (a) Leevy WM, Gammon ST, Jiang H, Johnson JR, Maxwell DJ, Marquez M, Piwnica-Worms D, Smith BD. J Am Chem Soc 2006;128:16476–16477. [PubMed: 17177377] (b) Leevy WM, Gammon ST, Johnson JR, Lampkins AJ, Jiang H, Marquez M, Piwnica-Worms D, Suckow MA, Smith BD. Bioconjugate Chem 2008;19:686–692.
19. Fragioni JV. Curr Opin Chem Biol 2003;7:626–634. [PubMed: 14580568]
20. Control 3 is the near-IR fluorophore, Indocyanine Green (ICG), which is approved for use in humans. It associates strongly with plasma proteins, and is rapidly cleared by the liver. ICG and non-targeted ICG-conjugates typically exhibit modest tumor targeting ability (T/NT < 2) due to enhanced permeation-retention (EPR) effects. See, for example: (a) Becker A, Riefke B, Ebert B, Sukowski U, Rinneberg H, Semmler W, Licha K. Photochem Photobiol 2000;72:234–241. [PubMed: 10946578] (b) Licha K, Riefke B, Ntziachristos V, Beckerm A, Chance B, Semmler W. Photochem Photobiol 2000;72:392–398. [PubMed: 10989611] (c) Perliz C, Licha K, Scholle FD, Ebert B, Bahner M, Hauff P, Moesta KT, Schirner M. J Fluoresc 2005;15:443–454. [PubMed: 15986163] For a recent serendipitous discovery of high ICG localization in human hepatocellular carcinoma, see: (d) Gotoh K, Yamada T, Ishikawa O, Takahashi H, Eguchi H, Yano M, Ohigashi H, Tomita Y, Miyamoto Y, Imaoka S. J Surg Oncol 2009;100:75–79. [PubMed: 19301311]
21. Pollard M, Suckow MA. Exp Biol Med 2005;230:520–526.
22. Bonnitcha PD, Vavere AL, Lewis JS, Dilworth JR. J Med Chem 2008;51:2985–2991. [PubMed: 18416544]
23. Kaijzel EL, van der Pluijm G, Lowik CWGM. Clin Cancer Res 2007;13:3490–3497. [PubMed: 17575211]
24. Direct comparison of ex vivo mean pixel intensities for probe 1 and control fluorophore 2 is possible because they have essentially identical brightness and the same fraction of light absorption/scattering by the excised tissue. The average ex vivo tumor intensity from rat dosed with probe 1 is 16-fold higher than rat dosed with control fluorophore 3 (ICG, see reference 20), however, this is only a qualitative measure of relative tumor selectivity because the brightness of 3 in tumor tissue is somewhat uncertain. As expected, the ex vivo imaging with probe 1 shows higher tumor selectivity than the in vivo imaging (T/NT) because fluorescence signal from the implanted tumor is attenuated by the surrounding skin and tissue.
25. At this point, we cannot rule out that a fraction of probe 1 is targeting the anionic epithelial cell surfaces that line the tumor vasculature. For further discussion of this possibility, see reference 10. Another topic for further study is whether probe 1 maintains its zinc(II) ions at the in vivo binding site. For evidence that this is the case in vitro, see: DiVittorio KM, Leevy WM, O'Neil EJ, Johnson JR, Vakulenko S, Morris JD, Rosek KD, Serazin N, Hilkert S, Hurley S, Marquez M, Smith BD. ChemBiochem 2008;9:286–293. [PubMed: 18076009]
26. (a) Loose D, Vermeersch H, De Vos F, Deron P, Slegers G, De Wiele CV. Eur J Nucl Med Mol Imaging 2008;35:47–52. [PubMed: 17906858] (b) Konstantinidou AE, Korkolopoulou P, Patsoursis E. J Neuro-Oncol 2005;72:151–156.
27. Brindle K. Nat Rev Cancer 2008;8:94–107. [PubMed: 18202697]
28. Weissleder R, Pittet MJ. Nature 2008;452:580–589. [PubMed: 18385732]

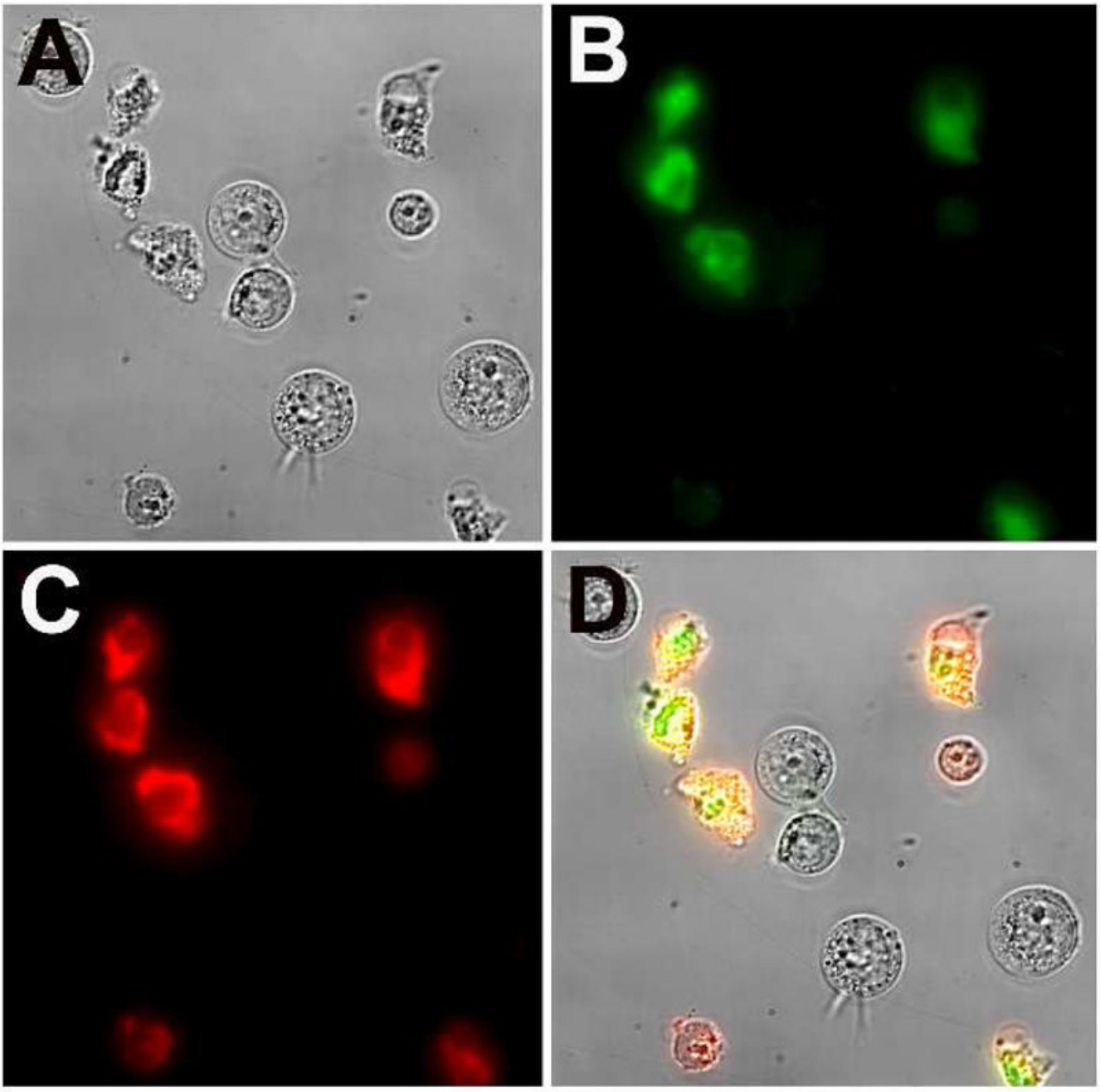

Figure 1.
Micrographs (60X magnification) of Jurkat cells treated with cytotoxic camptothecin (10 μM) for 3.5 h and stained simultaneously with Annexin V-Alexa Fluor 488, and probe **1** (10 μM). Brightfield image of the entire field of cells (A); cells stained with Annexin V-Alexa Fluor 488 (B); cells stained with probe **1** (C); overlay of images A, B, and C (D). No staining of healthy cells was observed in the absence of camptothecin.

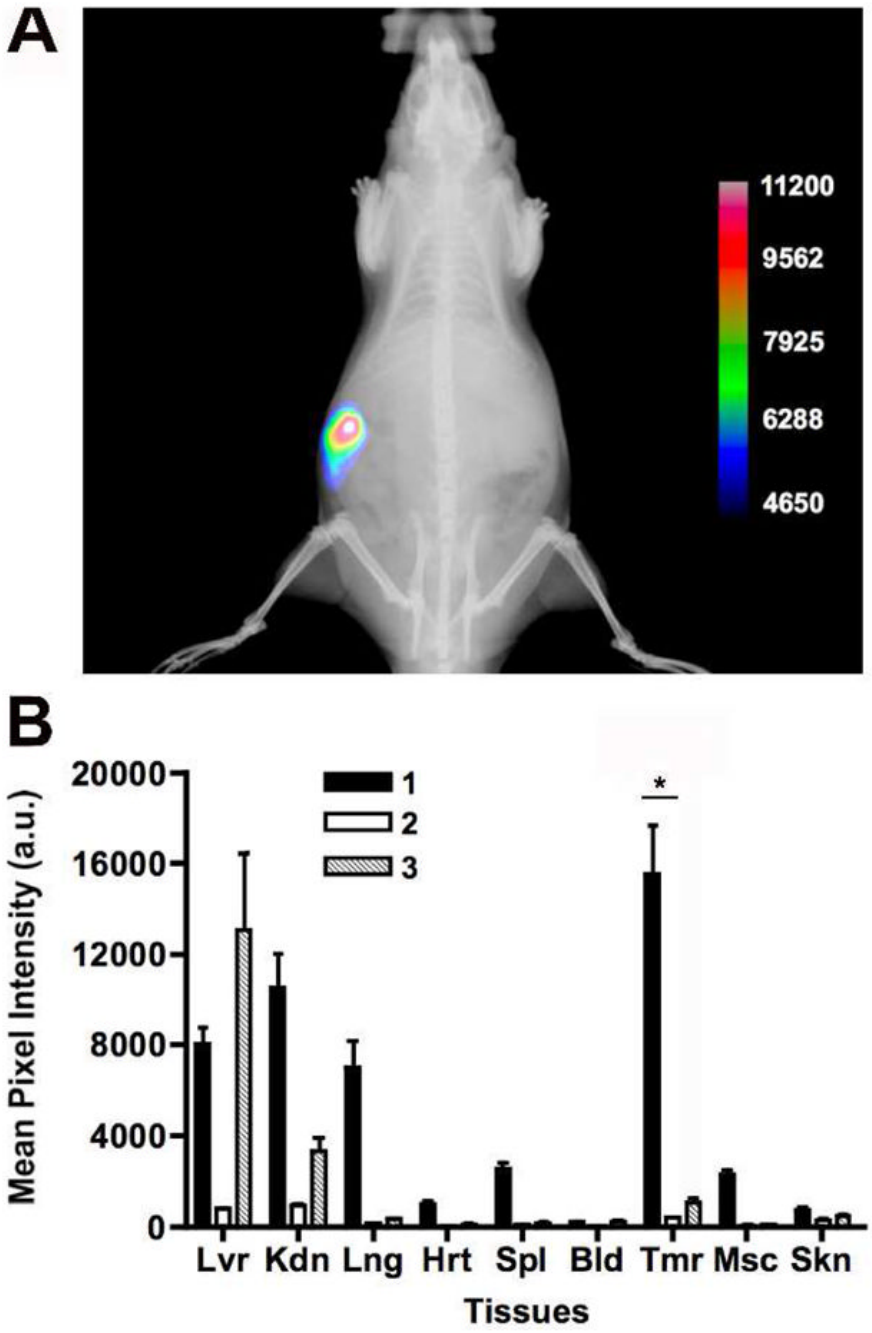

Figure 2.

X-ray and fluorescence overlay image of a rat prostate tumor model at 24 h post-injection of probe **1** (A). The image was acquired at a 190 mm field of view. Bar graph showing ex vivo tissue distribution of probes **1**, **2**, and **3** (B). The values represent the mean (n=3), ± standard error of the mean. *P<0.0005. This imaging data is representative of four replicate studies using independent cohorts.

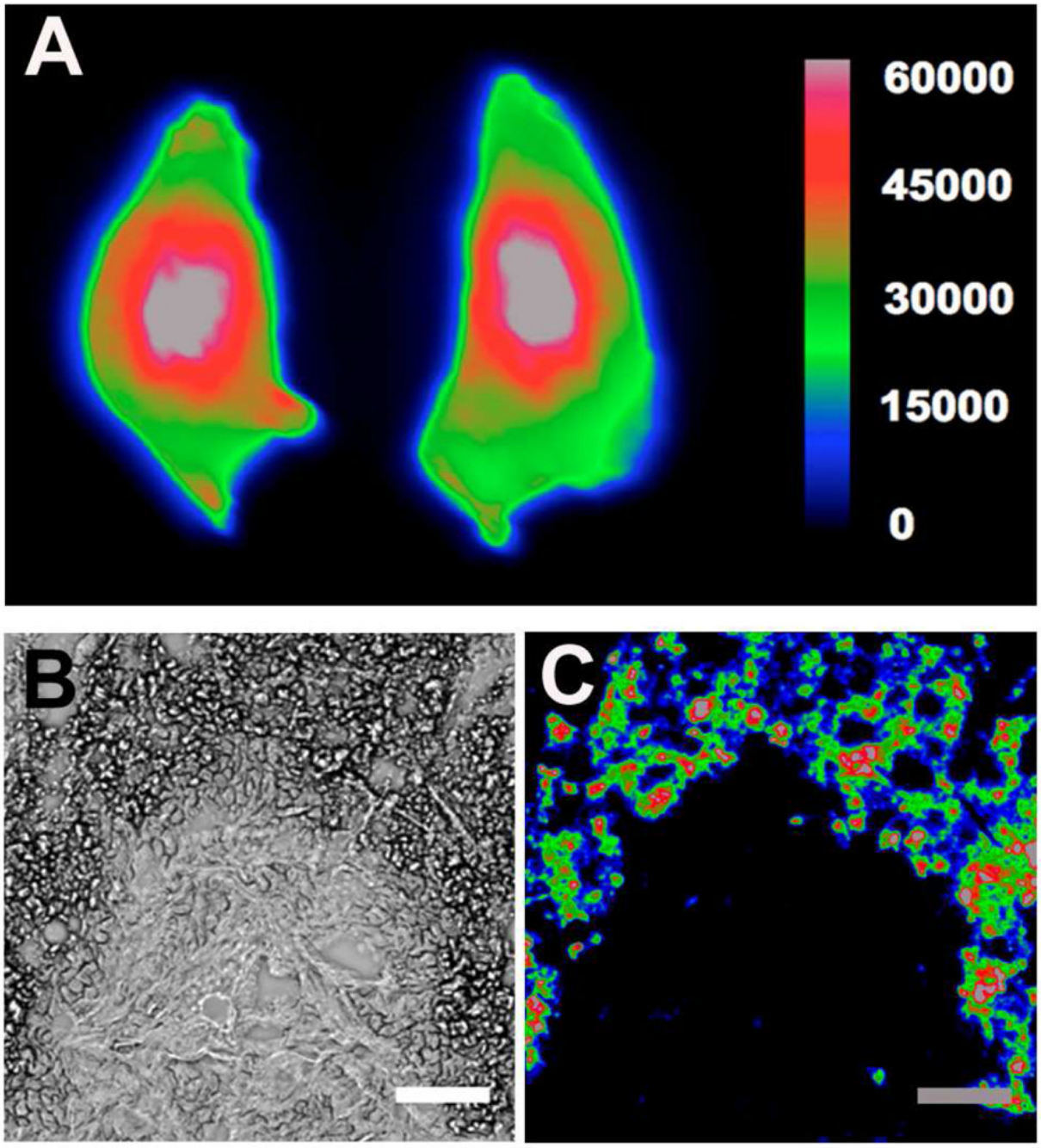

Figure 3.

Ex vivo analysis of probe **1** localization in rat prostate tumor. Excised PAIII prostate tumors were sliced along the longest axis, and a 30 mm field of view generated the representative near-IR fluorescence intensity image (A). Representative co-registered micrographs of a 5 μm histological slice of tumor core; the brightfield image (B) shows necrotic cells as darker regions that colocalize with near-IR fluorescence intensity image from probe **1** (C). Scale bar = 100 μm.

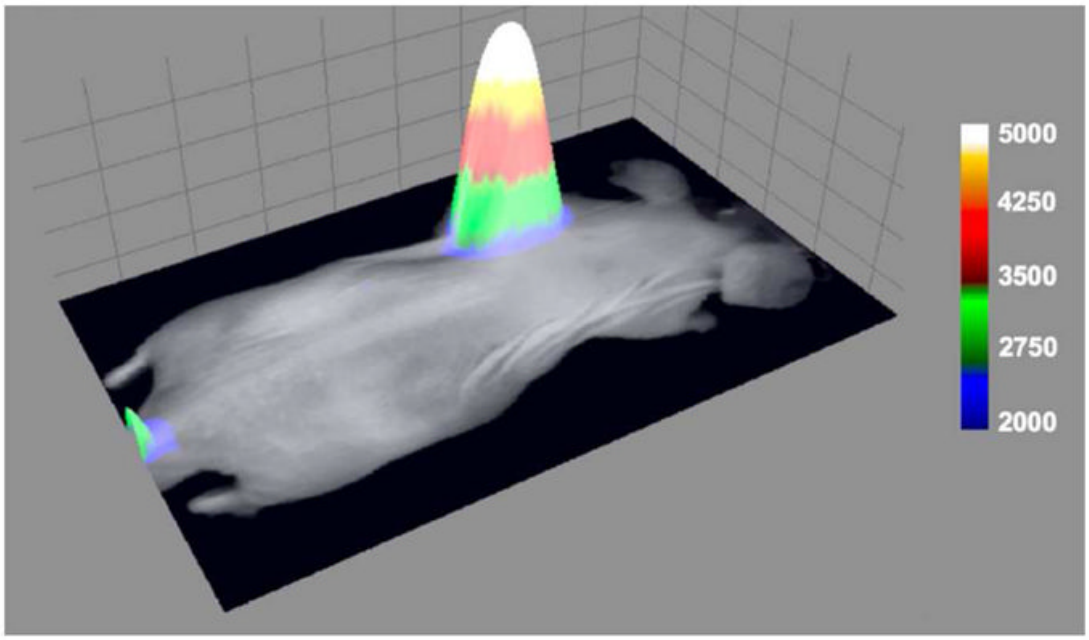

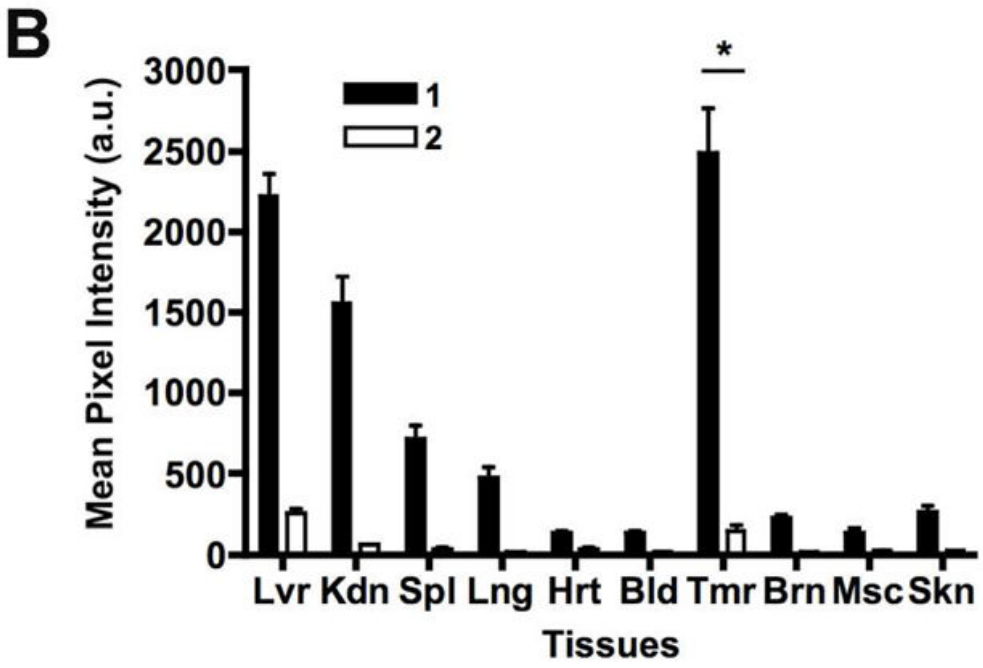

Figure 4.

Representative overlay image of a nude mouse with an EMT-6 mammary tumor. Brightfield and fluorescence intensity images were acquired 24 hrs following injection of probe **1** (A). The fluorescence intensity is plotted along the z-axis of this 3D surface diagram. Images were taken at an 80 mm field of view. Bar graph showing ex vivo tissue distribution of probe **1** and control **2** (B). The values represent the mean (n=3), ± standard error of the mean. *P<0.005. This imaging data is representative of three replicate studies using independent cohorts.